Liquid Crystals
Publication details, including instructions for authors and subscription information:
http://www.informaworld.com/smpp/title~content=t713926090

Conformational constraint in ferroelectric liquid crystals incorporating a pyrrolidine-type ring: FLC materials comprising parallel dipolar moments

Fernando Ely[ab]; Rodrigo Cristiano[a]; Ricardo L. Longo[c]; Rafael Vergara-Toloza[d]; Eduardo Soto-Bustamante[d]; Hugo Gallardo[a]
[a] Departamento de Química, Universidade Federal de Santa Catarina, 88040-900, Florianópolis, SC, Brazil [b] CenPRA, Centro de Pesquisas Renato Archer, DMI, Campinas, SP, Brazil [c] Departamento de Química Fundamental, Universidade Federal de Pernambuco, Recife, PE, Brazil [d] Universidad del Chile, Facultad de Ciencias Químicas y Farmacéuticas, Santiago, Chile

To cite this Article Ely, Fernando , Cristiano, Rodrigo , Longo, Ricardo L. , Vergara-Toloza, Rafael , Soto-Bustamante, Eduardo and Gallardo, Hugo(2007) 'Conformational constraint in ferroelectric liquid crystals incorporating a pyrrolidine-type ring: FLC materials comprising parallel dipolar moments', Liquid Crystals, 34: 4, 431 — 440
To link to this Article: DOI: 10.1080/02678290601171642
URL: http://dx.doi.org/10.1080/02678290601171642

Liquid Crystals, Vol. 34, No. 4, April 2007, 431–440

Conformational constraint in ferroelectric liquid crystals incorporating a pyrrolidine-type ring: FLC materials comprising parallel dipolar moments

FERNANDO ELY†‡, RODRIGO CRISTIANO†, RICARDO L. LONGO§, RAFAEL VERGARA-TOLOZA¶, EDUARDO SOTO-BUSTAMANTE¶ and HUGO GALLARDO*†

†Departamento de Química, Universidade Federal de Santa Catarina, 88040-900, Florianópolis, SC, Brazil
‡CenPRA, Centro de Pesquisas Renato Archer, DMI, Campinas, SP, Brazil
§Departamento de Química Fundamental, Universidade Federal de Pernambuco, 50740-540, Recife, PE, Brazil
¶Universidad del Chile, Facultad de Ciencias Químicas y Farmacéuticas, Santiago, Chile

(*Received 25 August 2006; accepted 8 November 2006*)

Ferroelectric liquid crystals bearing a chiral pyrrolidine-type ring were prepared using (–)-(*S*)-malic acid as a building block. The compounds were characterized using the thermal analysis techniques of DSC and POM, electrical measurements and temperature-dependent XRD. Samples showed moderate spontaneous polarization values (P_S) with helical pitches of about 2.997 μm and an average tilt angle of 16.2° for the SmC* planes. Conformational analysis of the chiral pyrrolidinol subunit and of all of the mesogenic targets was performed using several quantum methods including large basis sets and different treatments of electron correlation in order to correlate experimental results and theoretical predictions. For the most stable conformations, a very small dipole moment component perpendicular to the tilt plane was found which, according to the Boulder model, may be responsible for the moderate P_S values obtained.

1. Introduction

Ferroelectric liquid crystals (FLCs) with spontaneous polarization hold great potential in high-resolution microdisplay applications due to their fast response time, bistability and wide viewing angle; they are also potential candidates for nonlinear and photonic applications [1]. Spontaneous polarization is a chiral bulk property arising from a conformational preference for transverse molecular dipoles to orient in one direction along the polar axis because of steric coupling between polar functional groups and the chiral centre(s) in SmC* liquid crystals (stereopolar coupling). Lagerwall *et al.* [2] suggested some important factors that influence the dipolar order and promote a high level of polarization. Among them, a rigid steric coupling between the chiral centre and the molecular dipoles gives rise to stereopolar units (SPUs) and a slow intrinsic rotation of the dipoles attached to the chiral centre. Therefore, the strength of the spontaneous polarization ($\mathbf{P}_S$) can be increased considerably by restricting the freedom of rotation of the chiral centre with respect to the molecule as a whole. This can be achieved to some degree by moving the branch closer to the core, thus creating a direct interaction between them through a dipolar coupling and restricted rotation [3]. Restricted rotation has been achieved either by introducing bulk polar groups at the chiral centre, giving rise to larger energy differences between the conformations, or by incorporating the chiral centre into a cyclic system. Epoxides [4], thiiranes [5], lactones [6] and dihydrobenzofurans [7] are some examples of conformationally restricted systems that have been used in FLCs. The pyrrolidine structural unit is among the most commonly occurring structural cores, being found in a large number of biologically active alkaloids [8] and glycosidases [9], excitatory amino acid [10] and ACE inhibitors [11]. In addition to their medicinal importance, interesting examples of their use in asymmetric synthesis have been reported, including the stereoselective reduction of ketones [12] and asymmetric Diels–Alder reactions [13].

However, as far we know, there are no reports of the use of this five-member ring in liquid crystals. Moreover, from all the existing FLCs, how many of them possess a longitudinal dipole centre and chiral. To achieve this goal, first it is necessary to find the proper chiral centre. Second, the compound must exhibit

*Corresponding author. Email: hugo@qmc.ufsc.br

Liquid Crystals
ISSN 0267-8292 print/ISSN 1366-5855 online © 2007 Taylor & Francis
http://www.tandf.co.uk/journals
DOI: 10.1080/02678290601171642

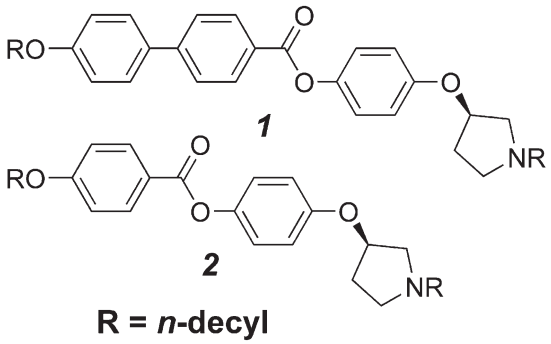

Figure 1. Molecular structure of the mesogenic compounds prepared.

mesophases and, third, the mesophases should have a tilted phase.

Thus, we now report an investigation on anisometric compounds containing a pyrrolidine-type chiral five-member ring. The main objective is to obtain ferroelectric SmC* phases and to analyse the effect of the conformational restriction imposed by the chiral portion on the $\mathbf{P}_S$. Figure 1 shows the mesogenic molecules synthesized for this study.

2. Results and discussion

2.1. *Synthesis*

In order to avoid any additional difficulty in achieving ferroelectric phases, the recognized SmC mesogenic cores biphenylbenzoate and phenylbenzoate were used, so that the effect of the chiral moiety could be better evaluated. Scheme 1 depicts the synthesis of the chiral pyrrolidinol **4** used in the preparation of **1** and **2**.

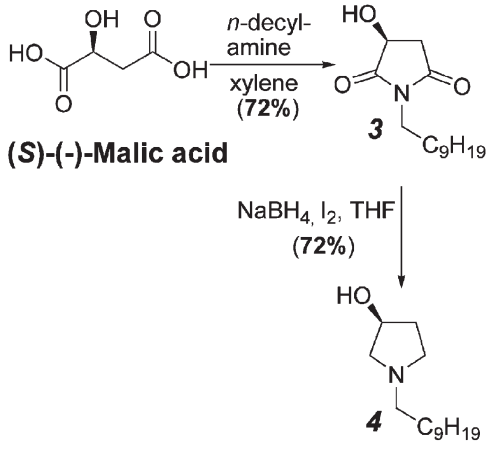

Scheme 1. Reactions involved in the synthesis of pyrrolidinol **4**.

Starting from (*S*)-(–)-malic acid, after condensation with *n*-decylamine and reduction of the corresponding pyrrolidinedione with borane, generated *in situ* from iodine and sodium borohydride, the desired chiral cyclic amino alcohol was obtained. The Mitsunobu reaction between the hydroquinone monobenzoate and **4** yielded the ether **5** with inversion of the configuration at the chiral centre. Deprotection by basic hydrolysis and subsequent esterification with the appropriate carboxylic acids yielded the target compounds **1** and **2**, according scheme 2.

2.2. *Liquid crystalline and ferroelectric properties*

Table 1 summarizes the transition temperatures for both compounds **1** and **2** from DTA measurements. Compound **1** is enantiotropic showing a paraelectric SmA and a ferroelectric SmC phase under heating and cooling. Compound **2** shows monotropic liquid crystalline behaviour with simultaneous occurrence of a paraelectric SmA and a ferroelectric SmC* phase under cooling. The phase assignment was carried out following texture evolution under a triangular wave form with a sufficiently low frequency of 1 Hz to observe the induced switching in the tilted SmC* phase at the phase transition.

In figure 2, typical optical photomicrographs for the SmC* phase for both compounds are displayed. For compound **1** (figure 2a), the texture was achieved applying 100 V_{pp} with a 100 Hz triangular wave to the sample at 160m°C in the SmC* phase. For compound **2** (figure 2b), a fan-shaped texture with an equidistant

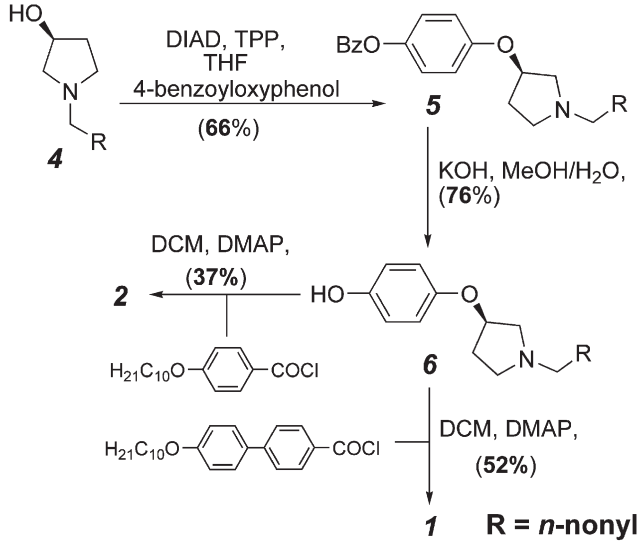

Scheme 2. Synthetic scheme for compunds **1** and **2**.

Table 1. Thermal behaviour of the pyrrolidine derivatives determined by optical microscopy and DSC (5°C min^{-1}).

Compound	Transition	T/°C, heating	T/°C, cooling
1	Cr–SmC*	97.1	91.4
	SmC*–SmA	166.2	161.8
	SmA–I	179.0	178.9
2	Cr–(SmC*)		42.6
	(SmC*)–(SmA)		75.2
	(SmA)–I	80.3	75.6

line pattern, due to the helical superstructure, was observed at 50.0°C, without an electric field. The helix conformation in the absence of an electric field is one of the most characteristic textures in FLCs bearing a chiral centre. From the several adjacent lines observed it was possible to estimate the pitch of the helix, which in this case was around 3 µm for sample **2**. Figure 2c shows the situation after several electro-optic cycles for this compound. At the left side of the electrode border, where the bias is applied, an electro-optic response is observed. At the right side, the region with no voltage treatment can be seen.

The experimental interlayer spacing, d, taken from X-ray measurements, is displayed in figure 3 for compound **1**. The temperature dependence of the first order reflection shows the existence of a nonlinear behaviour of the interlayer distance, with an exponential decrease under cooling from the isotropic state. The observed SmA to SmC change correlates reasonably well with the transition temperatures obtained by DSC.

Ferroelectric properties of the samples were determined according to the methods previously described in section 4. Figure 4 summarizes all switching times evaluated from the electric displacement curves and corresponding spontaneous polarization at different temperatures for compound **1**. The maximum $\mathbf{P}_S$ around 4.5 nC cm^{-2} is achieved at around 140°C. From figure 2a it is clear that the sample is not aligned, and hence $\mathbf{P}_s$ values measured will not be exact.

The polarization of compound **1** has a nonlinear behaviour with respect to temperature. The decrease in the pyroelectric signal is in good agreement with the increase in the time switching, at around 142°C, due to an increase in the viscosity of the mesophase at low temperature. For compound **2** the situation is different. It behaves as a monotropic liquid crystal, developing a short SmA phase followed by a SmC* phase before reaching the crystalline state. From figure 2c, can be seen the tendency of the sample to produce air bubbles, most probably due to the stress of the electric field applied. This situation was very difficult to overcome and therefore repolarization current experiments carried out on this compound were unsuccessful. From electrical field dependence pyroelectric measurements, not reported here, a spontaneous polarization varying from 1 to 8 nC cm^{-2} was indicated. From these measurements it

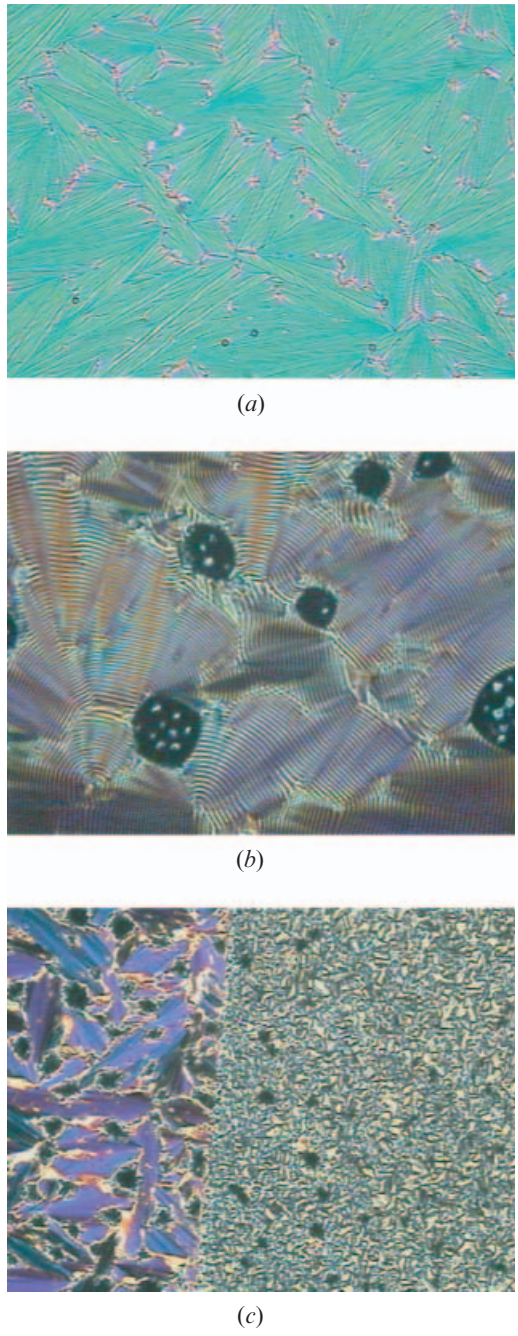

(*a*)

(*b*)

(*c*)

Figure 2. Observed texture of (a) compound **1**, smectic C* phase (T=160.0°C) with 100 V_{pp} electric field applied; (b) compound **2**, smectic C* phase (T=50.0°C), without electric field; and (c) texture at the electrode border interface (left side) for compound **2**.

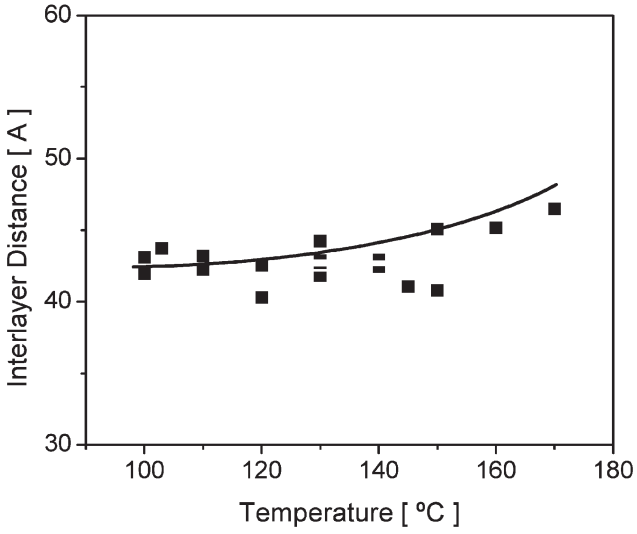

Figure 3. Temperature dependence of the interlayer distance *d* under cooling for compound **1**.

was clear that the sample has a strong ionic contribution to the observed polarization current.

2.3. *Conformational studies*

Pyrrolidine-type systems present several stable conformers usually described as envelope and half-chair structures [14], which are interconverted through ten pseudorotations with 36° increments (see figure 5).

Using *ab initio* calculations and electron diffraction experiments, the envelope conformation with the nitrogen atom out of plane and imino hydrogen in the axial direction has been found as the lowest energy conformer; this was corroborated by a microwave study [15]. However, when more accurate *ab initio* calculations were performed different results were obtained,

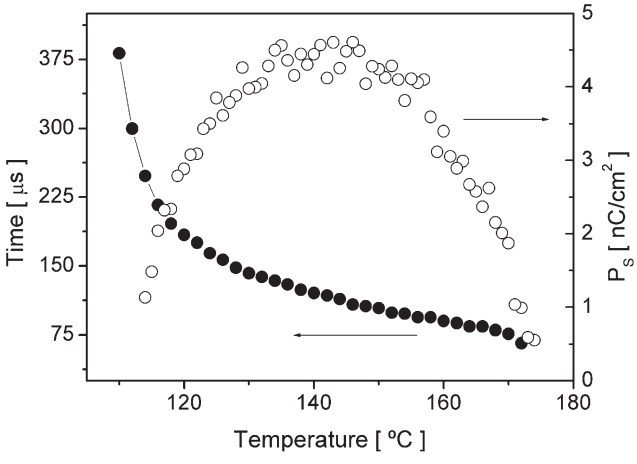

Figure 4. Temperature dependent switching time and spontaneous polarization for compound **1**.

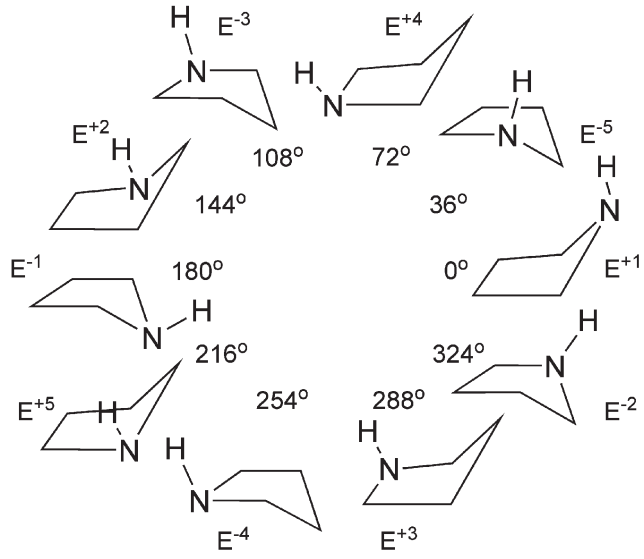

Figure 5. Envelope conformations along the pseudo-rotational path. There are ten twist conformations occurring between neighbouring envelope conformations.

namely, the MP2/6-31^{++}G** method indicated the *equatorial* envelope as the slightly more stable form, whereas the BLYP/6-31G** method yielded the *axial* as the global minimum [16]. In order to better understand the effect of the pyrrolidine ring on the experimental ferroelectric properties measured for compounds **1** and **2**, a series of computational quantum calculations was performed. First, we carried out a conformational analysis on the pyrrolidine ring to investigate the extent of the contribution of the chiral moiety to the $\mathbf{P}_S$ value in FLCs. Thus, the conformational behaviour of *N*-methyl-3-pyrrolidinol, the model compound for **4**, was investigated by means of a variety of theoretical methods. The methods included a large basis set and different treatments of electron correlation, i.e. B3LYP/6-31G*, B3LYP/6-311++G**, AM1 quantum chemical methods [17] and the MMFF94 [18] and MM+ [19] force fields. Figure 6 and table 2 summarize the results obtained for the most stable conformers and the respective energetics of the model compound *N*-methylpyrrolidine.

For the MMFF94 results, the equatorial *cis*-conformer that forms an intramolecular hydrogen bond was excluded from the analysis, since this conformer would not appear in the mesogen compounds. Clearly, the equatorial *trans*- and equatorial *cis*-conformers are the most stable ones. The relative stability is well reproduced by the B3LYP/6-31G* and MMFF94 methods (except for overestimation for the equatorial *cis*-conformer) when compared with the more accurate B3LYP/6-311++G** results. In contrast, the AM1 and

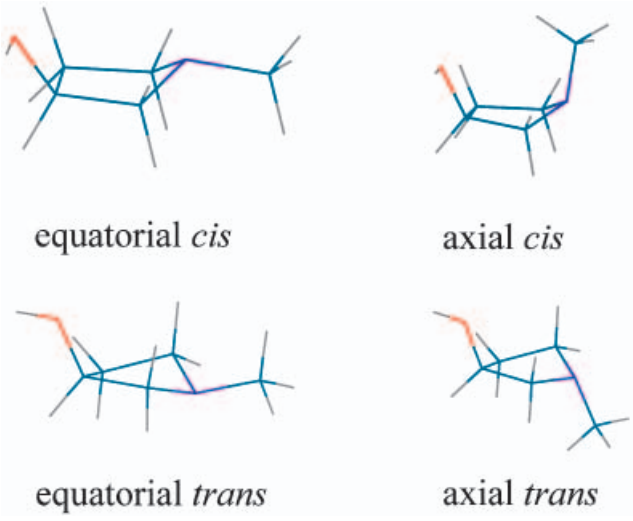

Figure 6. Most stable conformers calculated for *N*-methyl-3-pyrrolidinol, the model compound for **4**.

MM+ are unreliable methods for yielding the relative energies of the most important conformers. To provide a better model for validating the methodology, structures $\mathbf{M_1}$ and $\mathbf{M_2}$ (figure 7) were created from mesogens **1** and **2** by replacing the alkyl chains, $-C_{10}H_{21}$, at the phenoxy and *N*-pyrrolidine moieties with –H and $-CH_3$ groups, respectively.

Tables 3 and 4 show the calculated relative energies using different theoretical methods for the model compounds $\mathbf{M_1}$ and $\mathbf{M_2}$.

The relative energies of the conformers followed the trend observed for the *N*-methyl-3-pyrrolidinol, except for the AM1 results that improved quantitatively compared with the B3LYP/6-31G* results. However, just as in the case of *N*-methyl-3-pyrrolidinol, the AM1 method presents a significant failure by yielding practically planar pyrrolidine rings, which makes the distinction between equatorial and axial conformations meaningless. On the other hand, the MMFF94 method provided results in good agreement with the B3LYP method for geometries and relative energies. As a result, the molecular structure and relative energies of mesogens **1** and **2** were determined with the MMFF94 method. The methodology also needed to be validated in order to study the electrical properties of compounds **1** and **2**. The dipole moment and its components were calculated with B3LYP/6-31G* and AM1 methods for the geometry given by the former and with the MMFF94 method for its equilibrium geometry (see tables 5 and 6).

For both $\mathbf{M_1}$ and $\mathbf{M_2}$ the AM1 calculated dipole moments as well as their components are in very good agreement with the B3LYP/6-31G* results, whereas the

Table 2. Relative energies calculated (kJ mol^{-1}) for the most stable conformers of *N*-methyl-3-pyrrolidinol, model compound for **4**.

	Equatorial		Axial	
Method	*trans*	*cis*	*trans*	*cis*
B3LYP/6-31G*	0.0	2.66	14.14	12.21
B3LYP/6-311++G**	0.0	2.42	15.38	15.47
AM1	0.0	2.72	2.71	0.50
MMFF94	0.0	7.13	17.04	13.12
MM+	0.0	0.75	4.64	5.02

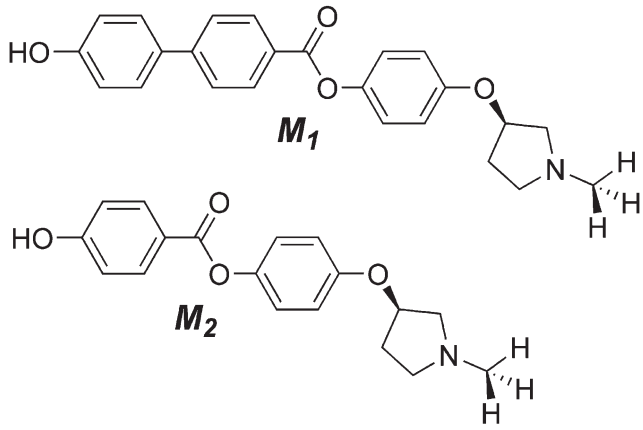

Figure 7. Chemical structures of $\mathbf{M_1}$ and $\mathbf{M_2}$, the model compounds for **1** and **2**, respectively.

Table 3. Calculated relative energies (kJ mol^{-1}) for the most stable conformers of $\mathbf{M_1}$, a model structure for **1**.

	Equatorial		Axial	
Method	*trans*	*cis*	*trans*	*cis*
B3LYP/6-31G*	0.0	1.61	8.56	5.06
AM1	0.0	4.35	7.24	6.19
MMFF94	0.0	7.00	8.41	7.03
MM+	1.97	2.68	0.0	15.44

Table 4. Calculated relative energies (kJ mol^{-1}) for the most stable conformers of $\mathbf{M_2}$, a model structure for **2**.

	Equatorial		Axial	
Method	*trans*	*cis*	*trans*	*cis*
B3LYP/6-31G*	0.0	2.05	8.22	4.93
AM1	0.0	3.90	7.24	6.32
MMFF94	0.0	7.02	8.45	6.77
MM+	2.04	2.61	0.0	4.15

Table 5. B3LYP/6-31G*, AM1 and MMFF94 calculated dipole moment, μ, and its Cartesian components (in parenthesis) for the conformers of $\mathbf{M_1}$. Values in debye.

	Equatorial		Axial	
Method	*trans*	*cis*	*trans*	*cis*
B3LYP/6-31G*	2.62 (1.94, 1.55, −0.86)	2.44 (−1.56, 1.82, −0.47)	2.24 (−1.63, 1.53, −0.13)	3.82 (2.30, −3.04, 0.01)
AM1	2.48 (1.82, 1.46, −0.83)	2.59 (−1.17, 2.30, 0.25)	2.20 (−1.25, 1.69, 0.64)	3.69 (2.07, −3.05, −0.03)
MMFF94	2.89 (2.53, 1.40, −0.04)	3.50 (−2.18, 0.41, −2.71)	3.20 (−2.61, 1.48, 1.12)	5.51 (2.72, −4.79, −0.22)

Table 6. B3LYP/6-31G*, AM1 and MMFF94 calculated dipole moment, μ, and its Cartesian components (in parenthesis) for the conformers of $\mathbf{M_2}$. Values in debye.

	Equatorial		Axial	
Method	*trans*	*cis*	*trans*	*cis*
B3LYP/6-31G*	1.96 (1.62, 1.04, −0.35)	1.86 (−1.22, 1.40, 0.12)	1.71 (1.41, −0.94, 0.28)	2.22 (2.06, −0.73, −0.39)
AM1	1.96 (1.68, 0.96, −0.30)	2.21 (−1.02, 1.77, 0.86)	1.99 (1.24, −1.20, 0.99)	2.15 (1.99, −0.69, −0.41)
MMFF94	2.89 (2.42, 1.57, −0.03)	3.50 (−2.13, 2.61, 0.93)	3.20 (2.63, 0.92, 1.57)	3.23 (2.78, −1.55, −0.58)

values of the MMFF94 results were systematically higher than those of the B3LYP/6-31G*. The values of the MM+ results for the dipole moments are not even given since they are systematically very low, with the highest being 0.3 D. As a result of this validation study, the MMFF94 method was chosen for the calculation of the molecular structure and conformational and energetic analysis of mesogens **1** and **2**; for these calculated geometries the AM1 method was used to estimate the dipole moment and its components.

Systematic and Monte Carlo searches for mesogens **1** and **2** were performed with the MMFF94 method and the most stable conformers were used as initial structures for creating the zigzag conformers, according to the Boulder model [20]. The equatorial *trans*- and equatorial *cis*-conformers were at least 15 kJ mol^{-1} more stable than all the other conformers. The Monte Carlo approach generated 5329 conformers for each starting conformation based upon the equatorial, axial, *cis*- and *trans*-structures. Some representative results for compound **1** are illustrated in figure 8.

Note that these most stable conformations have a very small dipole moment component perpendicular to the tilt plane ($\mu_\perp$) which, according to the Boulder model, is responsible for $\mathbf{P_S}$. In addition, these are coiled or bent conformations that should not correspond to the stable sites for a SmC* phase. Thus, the zigzag conformations were optimized and after reorientation along the largest inertia momentum axes the transverse dipole moment was calculated. The data obtained for **1** and **2** are shown in figure 9. Both mesogens show very similar behaviour, where the zigzag equatorial *trans*-conformers are the most stable ones and they have a very small transverse dipole component. Moreover, the equatorial *cis*-counterpart is less stable, but it has a large transverse dipole. This suggests that these energy differences are amplified in the SmC* which could explain the small $\mathbf{P_S}$ values observed in this phase for both **1** and **2** liquid crystals.

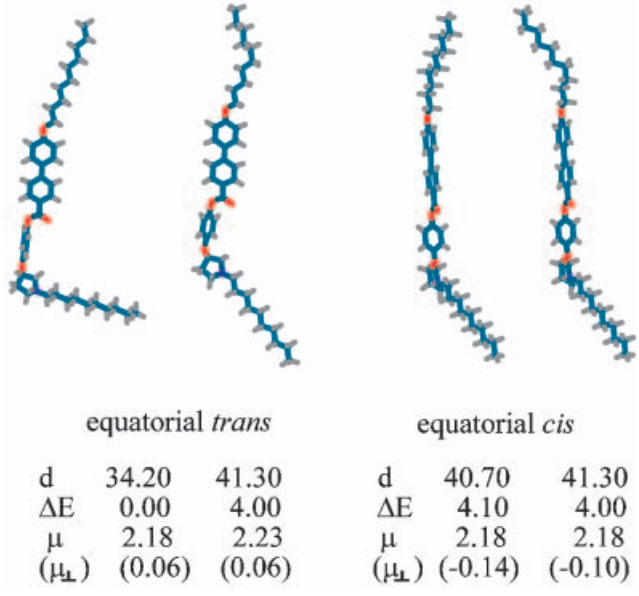

Figure 8. Representative conformers of **1**. Calculated structures (extremity distance *d* in Å) and energy differences (Δ*E* in kJ mol^{-1}) with MMFF94 and dipole moment (μ in D) and its perpendicular component ($\mu_\perp$ in D) with AM1.

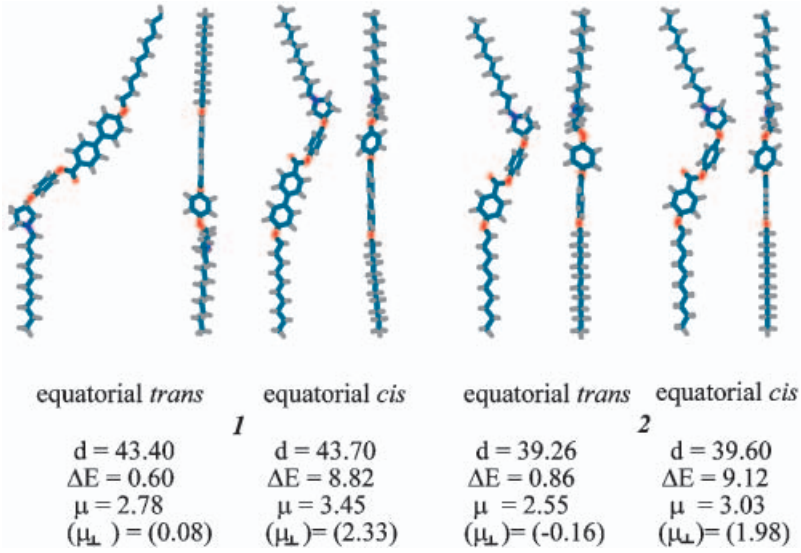

Figure 9. Representative conformers of **1** and **2** for the zigzag conformation. Calculated structures (extremity distance d in Å) and energy differences (ΔE in kJ mol^{-1}) with MMFF94 and dipole moment (μ in D) and its perpendicular component ($\mu_{\perp}$ in D) with AM1. The most stable conformer was taken as a reference for calculating the relative energies.

In addition, the calculated tilt angle for **1** at the zigzag equatorial *trans*-conformation (16.2°), assuming an average thickness of 42 Å (see figure 3) between the smectic planes, is slightly lower than the ideal angle (22.5°). For the non-zigzag conformers (figure 8) these tilt angles were found to be incompatible with the measured X-ray average interlayer distance.

These results thus corroborate the Boulder model results in explaining and/or predicting the electrical properties of FLCs. They also suggest that the energy differences obtained with the MMFF94 force field are quite reliable. From these calculations it is clear that in order to increase the $\mathbf{P}_S$ values of these mesogens it would be necessary to stabilize the equatorial *cis*- and/or destabilize the equatorial *trans*-conformations of the pyrrolidine ring through some substitution. This would also improve the transverse dipole of the active mesogen that should increase significantly.

Another result that corroborates the zigzag conformation for the mesogens in the SmC* phase is the energy differences calculated when aggregates comprising four mesogens are optimized (see figure 10). It can be seen that despite the isolated non-zigzag mesogen being slightly more stable than the zigzag conformer (0.6 kJ mol^{-1}, see figures 8 and 9), when a small aggregate is formed the zigzag conformation becomes dominant and much more stable.

3. Conclusions

The first example of a liquid crystalline system based on a pyrrolidine-type ring bearing a parallel dipolar moment directly linked to the aromatic core of a mesogen was successfully achieved. The compounds synthesized showed low values for spontaneous polarization, which may be related to the small contribution of the dipolar moment, achieved from the perpendicular component of the parallel dipole. The moderate values for spontaneous polarization are the result of this small contribution, also predicted theoretically in this study

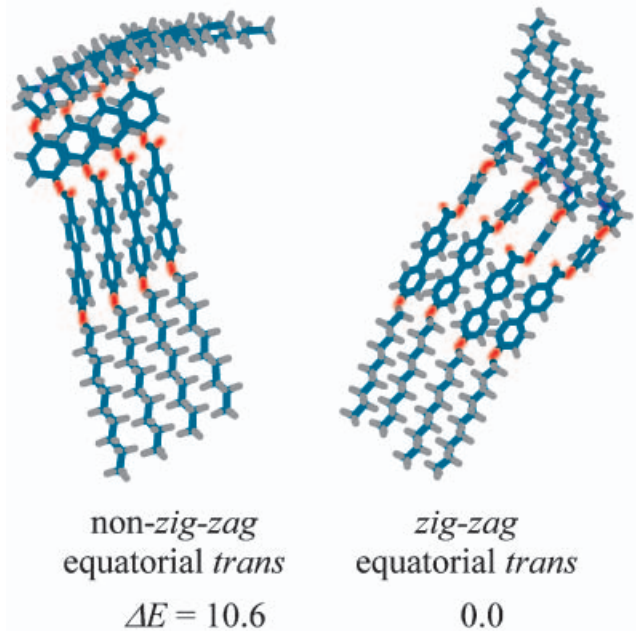

Figure 10. Relative energy (kJ mol^{-1}) of four interacting mesogens such as **1** in non-zigzag and zigzag conformations.

by computational methods. From these calculations it is clear that in order to increase the $\mathbf{P}_S$ of these mesogens it would be necessary to stabilize the equatorial *cis*- and/or destabilize the equatorial *trans*-conformations of the pyrrolidine ring through some substitution. However, the system may be of interest in the design of electric field-sensitive nematic phases, due to the lateral dipole disposition, and also for banana-shaped molecules, due to the possibility of improving the synclinic or anticlinic structure in such materials [21].

4. Experimental

4.1. *General*

^{1}H and ^{13}C NMR spectra were obtained with a Bruker AC-200F spectrometer at 200 MHz and 50.4 MHz, respectively, using TMS as the internal standard. IR spectra were recorded using KBr discs with a Perkin-Elmer model 283 spectrometer. Elemental analyses were carried out using a Perkin Elmer 2400 CHN analyser. Optical rotations were measured on a Perkin-Elmer 341 polarimeter at the sodium D line. The phase transition temperatures for the investigated samples were determined using a differential temperature analyzer (Mettler, FP90 DTA), with an accuracy of ± 0.1 K. A polarizing microscope (Leica, DLMP), equipped with a heating stage (HS-1, Instec) was used for temperature dependent investigations of liquid crystal textures. A video camera (Panasonic WVCP414P), installed on the polarizing microscope, was coupled to a video capture card (Miro DC-30) that allows real time video capture and image saving. The temperature dependence for the interlayer distance for one of the compounds was obtained using a horizontal two-circle X-ray diffractometer (STOE, STADI 2) with a linear position-sensitive detector [22, 23].

The ferroelectric liquid crystals were confined in commercial EHC KSRO-10 sandwich cells with a thickness of 11.5 μm and parallel alignment. They were filled by capillarity in the isotropic state. The cells were placed inside a temperature-controlled thermal oven (2, Instec MK2) that allows a temperature control ranging from $0.1^\circ\,\mathrm{min}^{-1}$ up to $20^\circ\,\mathrm{min}^{-1}$. The temperature range was from -170°C to 200°C. The heating or cooling process was monitored with an IBM-PC compatible computer. The electric displacement, D, was determined by the field reversal method [24]. A square wave voltage of 1 Hz frequency was applied to the sample cell and the electric displacement current was monitored on an oscilloscope HP 56000 linked to a PC computer through a GPIB card. The curves were stored in the PC for further data processing. The time switching was obtained directly from the time scale, at the polarization peak. The corresponding spontaneous polarization was determined using the triangular wave method [25], applying a voltage of 200 V_{pp} and 1 Hz to the sample cell. The polarization current, also followed with the oscilloscope and stored in the PC, can be easily obtained by subtracting the capacitive and ohmic components and taking into account the electrode areas.

4.2. *Materials*

All the reagents and chemicals were obtained from commercial sources and used without further purification unless otherwise noted. The organic solvents were of commercial grade quality except THF (HPLC grade) and all were dried by traditional methods. Analytical thin-layer chromatography (TLC) was conducted on Merck aluminium plates with 0.2 mm of silica gel 60F-254.

4.2.1. (3*S*)-1-*n*-Decyl-3-hydroxypyrrolidine-2,5-dione (3). (*S*)-(–)-Malic acid (20 g, 0.15 mol) and *n*-decylamine (29.6 ml, 0.15 mol) were suspended in xylenes (150 ml). A Dean–Stark apparatus was adapted for continuous water extraction. After 6 h the solvent was removed in a rotavapor at reduced pressure (1 mm Hg). The solid formed was purified by recrystallization from hexanes; yield: 68% of a white powder, m.p. 61.0–63.2°C. GC: capillary column chirasil-CB, temp. 300°C, R_t 8.09 min, single peak. $[\alpha]_D^{20} = -28.0$ (ca. 1.08, $CHCl_3$). ^{1}H NMR ($CDCl_3$) δ 0.88 (t, 3H), 1.25 (br, 14H), 1.57 (m, 2H), 2.65 (dd, J=18.2 and 4.8 Hz, 1H), 3.08 (dd, J 18.2 Hz and 8.4 Hz, 1H), 3.50 (t, 3H), 3.70 (br, 1H), 4.64 (dd, J=8.4 and 4.8 Hz, 1H).

4.2.2. (3*S*)-1-*n*-Decylpyrrolidin-3-ol (4). Imide **3** (11.6 g, 45.52 mmol) in dry THF (50 ml) was added to a slurry of $NaBH_4$ (9.3 g, 245.82 mmol) in THF (50ml). I_2 (27.74 g, 109.30 mmol) in THF (160 ml) was added dropwise under argon flux at 0°C for 5 h. The ice-water bath was removed and the mixture allowed to reflux for 18 h. After cooling at 0°C the excess hydride was carefully destroyed with 3M HCl (44.6 ml). When gas evolution ceased, the mixture was neutralized using 3M NaOH (117 ml). The organic layer was separated and aqueous layer extracted with ether and dried over sodium sulfate. The solvent was evaporated and the amine borane residue treated with methanol (75 ml) and concentrated HCl (11 ml). After gas evolution ceased, the solvent was evaporated. That treatment was repeated twice until the flame test did not show a green colour. Again, the residue was dissolved in methanol (75 ml) and KOH (2 g) and K_2CO_3 (75 g) was added. Methanol was evaporated and the solid was continuously extracted with ether

(700 ml) for 24 h. Evaporation under reduced pressure and vacuum distillation provided 7.0 g (72%) of the desired amino alcohol as a colourless oil, b.p. 129–131°C at 0.3 mm Hg. $[\alpha]_D^{20} = +5.9$ (ca. 1.01, $CHCl_3$). ^{1}H NMR ($CDCl_3$) δ 0.88 (t, 3H), 1.27 (br, 14H), 1.49 (m, 2H), 1.75 (m, 1H), 2.50 (m, 3H), 2.65 (m, 1H), 2.85 (m, 1H), 3.28 (br, 1H), 4.32 (m, 1H). ^{13}C NMR ($CDCl_3$) δ: 14.7; 23.3; 28.3; 29.3; 29.9; 30.2; 32.5; 35.5; 53.3; 57.1; 63.9; 71.7.

4.2.3. (3*R*)-4-(1-*n*-Decylpyrrolidin-3-yloxy)phenol (6). (i) *p-Hydroquinone monobenzoate*. Argon was continuously bubbled into a solution containing *p*-hydroquinone (16.5 g, 150 mmol), dichloromethane (100 ml) and dry pyridine (12.1 ml, 150 mmol). Benzoyl chloride (16.2 ml, 140 mmol) was added dropwise and stirring maintained for 3 h. The solvent was evaporated, water added and the mixture filtered, washing with water to remove unreacted *p*-hydroquinone. Ether (300 ml) was added to the solid material and the solution filtered. The filtrate was evaporated and the residue crystallized from ethanol/water providing a white powder. Yield: 16.27 g (51%), m.p. 162.7–165.5°C. IR (KBr) ν_{max}/cm^{-1}: 3455, 1713, 1597, 1508, 1339, 1281, 1269, 1220, 712. ^{1}H NMR ($CDCl_3$) δ 5.36 (broad, 1H), 6.83 (d, 2H), 7.04 (d, 2H), 7.54 (m, 3H), 8.18 (d, 2H). (ii) *Mitsunobu reaction*. Hydroquinone monobenzoate (1.01 g, 4.45 mmol), pyrrolidinol **4** (0.95 g, 4.45 mmol), triphenylphosphine (1.75 g, 6.67 mmol) and dry THF (15 ml) were mixed under flowing argon. Diisopropyl azodicarboxylate (1.05 ml, 6.67 mmol) in THF (10 ml) was added dropwise to the cooled solution (0°C). The ice-water bath was removed and stirring was maintained overnight. A few drops of water were added in order to destroy excess DAD. THF was evaporated and the resultant oil dissolved in hexane:ethyl acetate (7:3) (50 ml) and stirred overnight. The white solid was filtered off and the filtrate concentrated. Recrystallization from aqueous methanol of the residue furnished 1.24 g (66%) of the ether **5**, m.p. 60.5–65.7°C. (iii) *Benzoic ester hydrolysis*. The ether **5** (0.39 g, 0.92 mmol) was suspended in methanol:water (3:1) (12 ml). KOH (0.056g, 1.01 mmol) was added and the mixture stirred at room temperature for 4 h. The methanol was evaporated and the residue partitioned in ether/water and the phases separated. The aqueous layer was extracted with ether (2×15 ml) and the combined organic layers washed with saturated sodium bicarbonate solution (10 ml) and dried over sodium sulfate. The residue, after filtration and evaporation of the solvent, was recrystallized from heptane to furnish compound **6** as a white powder. Yield: 0.221 g (76%), m.p. 59.7–60.0°C, $[\alpha]_D^{20} = -13.0$ (ca. 1.00, $CHCl_3$). ^{1}H NMR ($CDCl_3$) δ 0.86 (t, 3H), 1.25 (br, 14H), 1.53 (m, 2H), 2.00 (m, 1H), 2.22 (m, 1H), 2.77 (m, 2H), 2.94 (m, 1H), 4.20 (br, 1H), 4.72 (m, 1H), 6.69 (q, J=9.1 Hz, 4H). ^{13}C NMR ($CDCl_3$) δ: 14.8, 23.4, 28.3, 29.0, 30.0, 30.2, 32.6, 53.6, 57.4, 61.0, 77.4, 117.0, 151.1, 151.8.

4.2.4. (3*R*)-4-(1-*n*-Decylpyrrolidin-3-yloxy)phenyl 4′-*n*-decyloxybiphenyl-4-carboxylate (1). The 4′-decyloxybiphenyl-4-carboxylic acid, previously prepared, (0.217 g, 0.63 mmol), dry dichloromethane (5 ml), freshly distilled $SOCl_2$ (0.07 ml, 0.94 mmol) and 3 drops of dry DMF were mixed and the mixture heated under reflux for 4 h. Volatiles were evaporated and the residual solid re-dissolved in dry CH_2Cl_2 (5 ml) and triethylamine (0.5 ml). A few crystals of DMAP were added. To the cold solution (ice/water) phenol **6** (0.210 g, 0.63 mmol) in dichloromethane (3 mL) was added dropwise. After complete addition the solution was stirred overnight under stirring; water was added and the phases separated. The aqueous layer was extracted with dichloromethane, and the combined organic extracts dried over sodium sulfate. After evaporation of the solvent the residue was recrystallized from ethanol giving 0.224 g (52%) of **1** as a white powder, $[\alpha]_D^{20} = -6.5$ (ca. 1.07, $CHCl_3$). IR (KBr) ν_{max}/cm^{-1}: 2921, 2857, 2788, 1727, 1601, 1504, 1288, 1260, 1195, 1088, 874, 761. ^{1}H NMR ($CDCl_3$) δ 0.87 (t, 6H), 1.27 (broad, 30H), 1.80 (m, 3H), 2.04 (m, 1H), 2.49 (m, 1H), 2.79 (m, 3H), 2.90 (m, 2H), 4.01 (t, J=6.4 Hz, 2H), 4.82 (m, 1H), 6.88 (d, 2H), 6.99 (d, 2H), 7.06 (d, 2H), 7.60 (d, 2H), 7.67 (d, 2H), 8.22 (d, 2H). ^{13}C NMR ($CDCl_3$) δ: 14.1; 22.7; 26.0; 27.6; 28.7; 29.3; 29.6; 31.9; 32.2; 53.1; 56.5; 60.4; 68.2; 114.9; 115.9; 122.5; 126.5; 127.6; 128.4; 130.7; 132.0; 144.4; 145.9; 155.5; 159.6; 165.5. Elemental analysis: calcd. for $C_{45}H_{65}NO_4$ C 79.02, H 9.58, N 2.05; found C 78.88, H 9.50, N 2.00%.

4.2.5. (3*R*)-4-(1-*n*-Decylpyrrolidin-3-yloxy)phenyl 4-*n*-decyloxybenzoate (2). This compound was synthesized according to the procedure described for **1**. Yield: 37% of a white powder (crystallized from ethanol/water), $[\alpha]_D^{20} = -6.0$ (*c* 1.00, $CHCl_3$). ^{1}H NMR ($CDCl_3$) δ 0.87 (broad, 6H), 1.27 (broad, 30H), 1.78 (m, 2H), 2.01 (m, 1H), 2.28 (m, 1H), 2.50 (m, 3H), 2.88 (m, 3H), 4.03 (t, J=6.4 Hz, 2H), 4.81 (m, 1H), 6.86 (d, J=8.5 Hz, 2H), 6.96 (d, J=8.5 Hz, 2H), 7.85 (d, J=8.5 Hz, 2H), 8.12 (d, J=8.5 Hz, 2H). ^{13}C NMR ($CDCl_3$) δ 14.1, 22.6, 25.9, 27.6, 28.7, 29.0, 29.3, 29.5, 31.9, 32.1, 53.0, 56.5, 60.3, 68.2, 76.7, 114.2, 115.8, 121.5, 122.5, 132.2, 144.4, 155.3, 163.4, 165.3. Elemental analysis: calcd. for $C_{39}H_{61}NO_4$, C 77.05, H 10.11, N 2.30; found, C 76.95, H 10.05, N 2.12%.

Acknowledgments

Dr Fernando Ely thanks the Fapesp agency for post-doc fellowship. This work was supported by the agencies CNPq-Brazil and Funcitec/SC and by the Pronex program. Rafael Vergara Toloza thanks MECESUP for a doctor fellowship.

References

[1] T. Matsumoto, A. Fukuda, M. Johno, Y. Motoyama, T. Yui, S.-S. Seomunc, M. Yamashitad. *J. Mater. Chem.*, **9**, 2051(1999); T.M. Hegmann, R. Meadows, M.D. Wand, R.P. Lemieux. *J. Mater. Chem.*, **14**, 185 (2004); R.P. Lemieux, R.P. *Accts Chem. Res.*, **34**, 845 (2001); J.A. Mc.Cubbin, X.R. Tong, Y.Z. Wang, V. Snieckus, R.P. Lemieux. *J. Am. chem. Soc.*, **126**, 1161 (2004); D.M. Walba. *Top. Sterochem.*, **24**, 457 (2003); E.A. Soto-Bustamante, S.V. Yablonsky, B.I. Ostrovskii, L.A. Beresnev, L.M. Blinov, W. Haase. *Chem. Phys. Lett.*, **260**, 447 (1996); S.V. Yablonskii, E.A. Soto-Bustamante, R.O. Vergara-Toloza, W. Haase. *Adv. Mater.*, **16**, 1936 (2004).

[2] S.T.B. Lagerwall, B. Otterholm, K. Skarp. *Mol. Cryst. liq. Cryst.*, **152**, 503 (1987).

[3] J.W. Goodby, T.M. Leslie. *Mol. Cryst. liq. Cryst.*, **110**, 175 (1984).

[4] D.M. Walba, H.A. Razavi, N.A. Clark, D.S. Parmar. *J. Am. chem. Soc.*, **110**, 8686 (1988).

[5] J.W. Goodby. In *Handbook of Liquid Crystals* Vol 2B, J.W. Goodby, D. Demus, G.W. Gray, H.-W. Spiess, V. Vill (Eds), Wiley-VCH, Weinheim (1998).

[6] T. Ikemoto, Y. Kageyama, F. Onuma, Y. Shibuya, K. Ichimura. *Liq. Cryst.*, **17**, 729 (1994).

[7] H. Matsutani, K.-I. Sato, T. Kusumoto, T. Hiyama, S. Takehara, H. Takezoe, T. Furukawa. *Mol. Cryst. liq. Cryst.*, **263**, 131 (1995).

[8] W.H. Pearson. In *Studies in Natural Product Chemistry* Vol. 1, A.U. Rahman (Eds), Elsevier, Amsterdam (1988).

[9] M. Lombardo, S. Fabbroni, C. Trombini. *J. org. Chem.*, **66**, 1264 (2001).

[10] R.J. Bridges, F.E. Lovering, J.M. Humphrey, M.S. Stanley, T.N. Blakely, M.F. Cristopharo, A.R. Chamberlin. *Bioorg. Med. Chem. Lett.*, **3**, 115 (1993).

[11] E.W. Petrillo, M.A. Ondetti. *Med. Res. Rev.*, **2**, 1 (1982).

[12] E.J. Corey, R.K. Bakshi, S.J. Shibata. *J. Am. chem. Soc.*, **109**, 5551 (1987).

[13] S. Kobayashi, M. Murakami, T. Harada, T. Mukaiyama. *Chem. Lett.*, 1341 (1991).

[14] A.C. Legon. *Chem. Rev.*, **80**, 231 (1980).

[15] G. Pfafferott, H. Oberhammer, J.E. Boggs, W. Caminati. *J. Am. chem. Soc.*, **107**, 2305 (1985).

[16] B. Velino, A. Millemaggi, A. Dell'Erba, W. Caminati. *J. Mol. Struct.*, **599**, 89 (2001).

[17] C. Cremer. In *Essential Computational Chemistry*. Wiley, New York (2003).

[18] T.A. Halgren. *J. Comput. Chem.*, **17**, 490, 520, 553 (1996).

[19] N.L. Allinger. *J. Am. chem. Soc.*, **99**, 8127; HyperChem version 6.0, Hypercube, Inc., Gainesville, FL (1977).

[20] D.M. Walba. In *Advances in the Synthesis and Reactivity of Solids*, pp. 173–235, T.E. Mallouck (Ed.), JAI Press, Greenwich (1991).

[21] T. Niori, T. Sekine, J. Watanabe, T. Furukawa, H. Takezoe. *J. Mater. Chem.*, **6**, 1231; D.R. Link, G. Natale, R. Shao, J.E. Maclennan, N.A. Clark, E. Körblova, D.M. Walba. *Science*, **278**, 1924 (1997) (1996).

[22] W. Klämke, Z.X. Fan, W. Haase, H.J. Müller, H.D. Gallardo. *Ber. Bunsenges. Phys. Chem.*, **93**, 478 (1989).

[23] Z.X. Fan, W. Haase. *J. chem. Phys.*, **95**, 6066 (1991).

[24] W.J. Merz. *J. appl. Phys.*, **27**, 938 (1956).

[25] K. Miyasato, S. Abe, H. Takezoe, A. Fukuda, E. Kuze. *Jap. J. appl. Phys.*, **L661**, 22 (1983).